4th Imeko TC 19 Symposium on Environmental Instrumentation and Measurements
Protecting Environment, Climate Changes and Pollution Control
June 3-4, 2013, Lecce, Italy

AN ARTIFICIAL NEURAL NETWORK APPROACH TO INVESTIGATE CAVITATING FLOW REGIME AT DIFFERENT TEMPERATURES

M.G. De Giorgi[a,b], *D. Bello*[a,c], *A.Ficarella*[a,d]

[a] Dep. of Engineering for Innovation, University of Salento, Via per Monteroni, Lecce – Italy,
[b]mariagrazia.degiorgi@unisalento.it; [c]daniela.bello@unisalento.it; [d]antonio.ficarella@unisalento.it

Abstract: The aim of the present study is to implement an useful approach to predict and on-line monitoring the cavitating flow and to investigate the influence of the different parameters on the phenomenon by the application of Artificial Neural Network (ANN). A three-layer Elman neural network was designed, using as inputs the power spectral density distributions of dynamic differential pressure fluctuations, recorded downstream and upstream the restricted area of the orifice. The results show that the designed neural networks predict the cavitation patterns successfully comparing with the cavitation pattern by visual observation. The Artificial Neural Network underlines also the impact that each input has in the training process, so it is possible to identify the frequency ranges that more influence cavitation regimes and the impact of fluid temperature.

Keywords: cavitation; artificial neural network; image visualization; thermal effect.

1. INTRODUCTION

Cavitation is a very complex problem, that occurs in a large number of hydraulic machines, e.g. pumps, turbines, rockets, internal combustion engines and injection systems. It negatively affects the performance of many machines and can damage materials and induce vibrations.

In presence of cavitation, cavities filled with water vapour are formed; once the vapour bubbles reach higher pressure regions on their paths they collapse by an implosion, so tiny pits or craters damage the solid surface. Otherwise there are some applications where cavitation phenomenon increases the efficiency, e.g., atomization downstream of injector nozzles of diesel engines can be improved by evaporation of the fuel before injection [1, 2, 3]. So, in this case to improve the atomization a cavitation control and further understanding of cavitation are necessary.

Moreover, two-phase regime depends on several parameters as operating pressure and temperature. Thermal effects could be important in some cases including hot fluid injection, cryogenic fluids, and flow in the feeding system of a liquid rocket. Few experimental works have been performed to investigate the influence of thermal effects on cavitation onset and development in internal flows [4, 5, 6, 7, 8] focusing on temperature depression in the vapour region. In the present work, attempts have been made to extend the knowledge on flow regime transitions due to cavitation in an orifice in presence of thermosensible fluids, i.e., hot water.

At high temperature, the temperature gradient between the two phases, liquid and vapour, influences the vapour pressure in the cavities, i.e., their growth and collapse. Due to thermal effect, the vapour pressure is lower than that in absence of thermodynamic effects.

In the present work, attempts have been made to extend the knowledge on unsteady behaviour of two phase flow and regime transitions due to cavitation in an orifice in presence of thermosensible fluids, i.e., hot water [10].

The identification of cavitation regime is a basic and important issue in multiphase systems, especially considering that in many cases flow visualization is impossible.

In the present work Artificial Neural Network (ANN) were applied to cavitation in an orifice, with two aims: the first purpose was to shown their potential application to on-line monitoring and diagnostics; the second one was to better understand the phenomenon and to underline the role of the different parameters, as temperature and characteristic flow frequencies, on the development of the cavitation structures. A three-layer Elman neural network was designed, using as inputs the power spectral density distributions of dynamic differential pressure fluctuations, recorded downstream and upstream the restricted area of the orifice.

2. EXPERIMENTAL FACILITY

In the present work a water cavitating orifice has been investigated under different flow conditions.

The experimental setup is described in [11, 12, 13, 14].

The test data are available for a transparent acrylic sharp-edge orifice. The test section has a circular pipe $11.25e^{-3}$ *m* in diameter (D) and an internal circular cylindrical orifice with a diameter (d) of $2.5e^{-3}$ *m* and a length L = $7.5e^{-3}$ *m*.

The signals of two Kistler 4045A piezoresistive pressure sensors were acquired at a sampling rate of 102000 *Hz* for each channel, up and downstream of the test section pressure. The accuracy of pressure measurement is with an uncertainty of $+/-0.003MPa$.

The pressure signals were analyzed using a Labview ® based routine. The routine calculated the fast Fourier transform FFT of the pressure fluctuations after subtracting

the signal mean value. The FFT, shown below, was calculated as an average of twenty FFTs, each performed on a hanning windowed signal lasting $0.1s$.

Images of cavitating flow pattern were recorded using a high-speed CCD camera (Kodak Motion Corder Analyzer FASTCAM - Super $10k$). For each of experimental test 300 images were acquired at a frequency of $2000Hz$.

The mass flow rates, measured by a flow meter upstream of the test section, and the pressure upstream of the test section were set by two calibrated control valves.

Experimental cavitation number was defined as:

$$\sigma = \frac{p_0 - p_v}{p_0 - p_{out}} \qquad (1)$$

where p_0, p_v, and p_{out} are, respectively, the inlet, vapour and outlet pressure. Experimental cavitation number, σ, is calculated using the pressure sensor measurements, with an uncertainty of the order of ± 0.04 at Reynolds number equal to $5 \cdot 10^4$.

The different operating conditions have been tested.

3. CAVITATING FLOW REGIMES

By the visualizations four cavitating flow regimes, from inception to developed cavitation, supercavitation and jet cavitation, can be identified at different cavitation numbers and fluid temperature, as shown in Fig. 1.

At high cavitation number, a cavitation cloud was evident in correspondence of inlet orifice, just downstream of the vena contracta. By lowering cavitation number, flow pattern moved to developed cavitation, where a rapid cavitation length increase was evident. With a further decrease in the cavitation number, the general aspect of cavitation cloud inside the orifice did not change, even when its optical "consistency" increased, given by the white level related to bubble density. This stage is called supercavitation.

Due to a further decrease in the cavitation number, an increasing portion of the cavitation cloud was carried by the flow out of the restricted area of the orifice. This is the next stage of the cavitation phenomenon, related to the transition to jet cavitation.

Tab. 1 presents the cavitation numbers that characterize the transition between different flow patterns.

By increasing the temperature in the range $293 - 333K$ range, the incipient cavitation appeared at a higher cavitation number; a further increase of liquid temperature, to $348K$, caused a decrease in the cavitation number at which cavitation starts. The transition to supercavitation regime is more affected by temperature: the thermodynamic effects became more evident as the cavitation number decreased. A study of the amplitude signal variation coupled with the image analysis permits for the unique identification of the threshold value of the two-phase flow regime.

An examination of the amplitude of the FFT frequency spectrum demonstrates the presence of different dominant frequencies in the $0 - 10000$ Hz range. In Fig. 2 the square underlined the most dominant frequencies ranges at different cavitation regimes.

The amplitude spectra of the down- and upstream pressure signals indicate that at high cavitation numbers (incipient cavitation and developed cavitation regimes), the FFT amplitude of the upstream pressure was higher than the downstream especially in the high frequency range due to the growth and collapse of small cavities.

Lowering cavitation number the spectra of the upstream signals show no evident peaks, and there is an increase in the FFT amplitude of the downstream signals in the $0 - 2000$ Hz frequency range, which is due to an increase in vapour cavity volumes and collapse time.

Tab. 1: Cavitation behavior at different temperatures T_∞ and cavitation numbers σ

T	*nocav→developing*	*developing→super*	*super→jet*
293	2.16	1.94	1.58
333	2.34	2.09	1.80
348	2.24	1.90	1.75

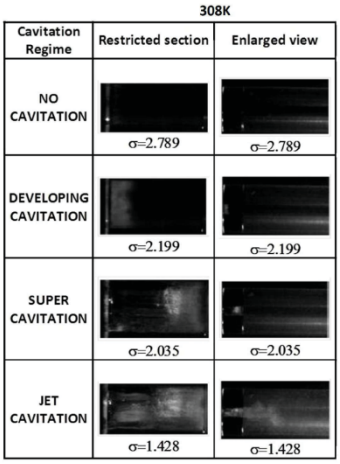

Fig. 1: Cavitation behavior in the restricted section of the sharp-edged orifice and in a larger view for different cavitation numbers at T_∞= 308K

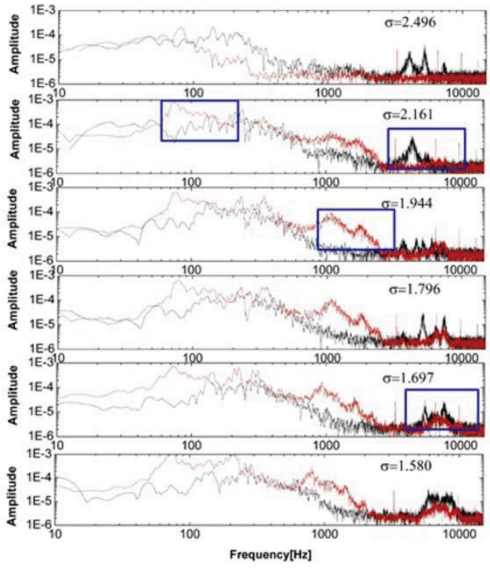

Fig. 2: Amplitude spectrum of the downstream (red line) and upstream (black line) pressure fluctuations at T = 293K and different cavitation numbers

4. ANALYSIS OF CAVITATING REGIME BY ARTIFICIAL NEURAL NETWORK

A three-layer Elman artificial neural network (ANN) was implemented both to demonstrating the potential application to on-line monitoring and diagnostics of cavitation, as well as to better understanding the relationship between some parameters, as temperature and characteristic flow frequencies, to the cavitating flow regime.

This ANN is characterized by feedback from the first-layer output to the first layer input. This recurrent connection allows the Elman network to both detect and generate time-varying patterns [15;16].

A *back-propagation* training algorithm was used. The goal of the algorithm is to minimize the global error *E* defined as

$$MSE = \frac{1}{2}\sum_{k=1}^{n}\big(t(k) - o(k)\big)^2 \qquad (2)$$

where $t(k)$ and $o(k)$ are respectively target and output network value for any *k* output node.

The power spectral density function is used to characterize the cavitating flow, by a parameterization of the data contained in the spectral domains, as reported in [17]. The frequency range over $0 - 10000\ Hz$ is divided into twenty bandwidths for each sensor (downstream and upstream pressure sensors) as shown in Tab. 2.

To approximate the percentage of energy the signal has in a given frequency band, the estimated average power spectral density was summed over the desired frequency band, respectively denoted as $\overline{P_{B1d}}$, ⋯, $\overline{P_{B20d}}$ for the downstream signals frequency and $\overline{P_{B1u}}$, ⋯, $\overline{P_{B20u}}$ for the upstream signals frequency.

The average values of power in each of the bands is used as a representative of the individual band. Other parameters of interest are the dominant frequency f_{DOM} in the power spectrum, and the spectrum variance, estimated from:

$$f_{DOM} = \sum_i f_i \cdot P_x(f_i) / \sum_i P_x(f_i) \qquad (3)$$

and

$$\sigma_f^2 = \sum_i (f_i - f_{DOM})^2 \cdot P_x(f_i) / \sum_i P_x(f_i) \qquad (4)$$

where σ_f^2 is the spectrum variance, $P_x(f_i)$ is the power spectral density for the i input and f_i is the frequency.

Each dominant frequency and spectrum variance is calculated for downstream and upstream pressure signals.

The above discrete parameters, representing the characteristics of power spectrum of pressure fluctuations, and temperature values were adopted as the 45 inputs of the neural networks.

The output of the neural network is an indicator of cavitation regime. Based on literature ([17]), the no-cavitation, developing, super and jet cavitation regimes are described, respectively, by the target output values 0.3, 0.5, 0.7 and 0.9 . The different regimes are therefore treated as an ordinal variable, with values based on the observed typical sequence of pattern transitions.

Tab. 2: Frequency band

Band name	*Frequency Range*	*Average Power*
B1	0 – 100	$\bar{P}_{B1}$
B2	100 – 200	$\bar{P}_{B2}$
B3	200 – 300	$\bar{P}_{B3}$
B4	300 – 400	$\bar{P}_{B4}$
B5	400 – 500	$\bar{P}_{B5}$
B6	500 – 600	$\bar{P}_{B6}$
B7	600 – 700	$\bar{P}_{B7}$
B8	700 – 800	$\bar{P}_{B8}$
B9	800 – 900	$\bar{P}_{B9}$
B10	900 – 1200	$\bar{P}_{B10}$
B11	1200 – 1500	$\bar{P}_{B11}$
B12	1500 – 2000	$\bar{P}_{B12}$
B13	2000 – 3000	$\bar{P}_{B13}$
B14	3000 – 4000	$\bar{P}_{B14}$
B15	4000 – 5000	$\bar{P}_{B15}$
B16	5000 – 6000	$\bar{P}_{B16}$
B17	6000 – 7000	$\bar{P}_{B17}$
B18	7000 – 8000	$\bar{P}_{B18}$
B19	8000 – 9000	$\bar{P}_{B19}$
B20	9000 – 10000	$\bar{P}_{B20}$

The output value from the neural networks is continuous, and 0.4; 0.6 and 0.8 were set a priori as the decision boundaries between the flow patterns. To identify the best Neural Network to predict the cavitation phenomenon, calculation of the MSE (%) between the numerical values corresponding to the identified and observed cavitation regimes is calculated.

The neurons in the input and the hidden layer have a hyperbolic tangent sigmoid transfer function, while the neurons in the output layers used the linear transfer function. The back-propagation learning algorithm was used.

The training process is made up of a test set including the fluid temperature among the inputs, while the other inputs are the above described values of $\overline{P_{B1}}$, $\overline{P_{B2}}$, ⋯,$\overline{P_{B20}}$, f_{DOM} and σ^2 for upstream and downstream pressure sensors.

So 478 groups of normalized dynamic differential pressure data at the above specified temperatures were available for the neural networks.

Following a common practice, a fraction of the obtained data was selected for training the neural networks, which constituted the so-called training data. The remainder of the data (139 data records), which the network had never "seen" during the training process, was used to test the network. The test set of data was of course randomly chosen to avoid a memorized-patterns effect. The training and test of the neural networks were programmed using the software package MATLAB 7 ®.

To verify the performance of the ANN in the identification of the possibility factor F_P is used, the parameter is defined as:

$$F_P = (1 - |Y_O - T_T|) \cdot 100 \qquad (5)$$

where Y_O and Y_T, respectively, denote the neural network output and its target output, and $0 < F_P < 1$. The value of the target output in Tab. 3 is determined by the high speed visualization.

Tab. 3 shows that high cavitation regimes, that means low cavitation number, are better predicted at low temperature, because at higher temperature the thermal effects reduce development of the cavitation phenomenon.

Tab. 3: Prediction results of the cavitation regime in the best proposed neural network (1000 epochs, 200 second layer neurons) at different temperatures

Target cavitation pattern	F_p (Possibility Factor) [%]	
	T=293K	T=348K
0.3	*0.90232*	*0.92879*
0.5	*0.98171*	*0.83792*
0.6	*0.94175*	*0.89729*
0.7	*0.94372*	*0.662*
0.8	*0.866*	*0.90573*
0.8	*0.8976*	*0.95952*
0.8	*0.97617*	*0.92353*
0.9	*0.93701*	*0.78035*
0.9	*0.96154*	*0.79685*
0.9	*0.93279*	*0.81733*
0.9	*0.99861*	
0.9	*0.97722*	
0.9	*0.976*	
0.9	*0.9331*	
0.9	*0.7895*	

A very important parameter to evaluate the influence of each parameter on the training of the neural network is the effectiveness factor α_i (Eq. 6) of each input on the model output.

This parameter is defined as in [18]:

$$\alpha_i = \xi_i / \sum_{j=1}^{n} \xi_i \tag{6}$$

$$\xi_i = \frac{1}{M} \sqrt{\sum_{j=1}^{M} \frac{F(I_1(j), I_2(j), \cdots \bar{I}_i(j), \cdots I_n(j))}{F(I_1(j), I_2(j), \cdots I_n(j))}} \tag{7}$$

where $F(I_1(j), I_2(j), \cdots I_n(j))$ is the output of the neural network model with the input of $I_1(j), I_2(j), \cdots I_n(j)$ and n is the total number of inputs. $\bar{I}_i(j)$ is the average of $I_i(j)$, $j = 1, 2, \cdots, M$ where M is the total number of samples.

In Fig. 3 the effectiveness factor evaluated over the whole experimental data set, using both the downstream (P_{bid}) and upstream (P_{biu}) pressure signals is shown. The variance was the first largest impacts on the cavitation pattern prediction, due to the presence of several different frequencies components in the entire process of cavitation development.

Looking to the frequencies ranges the major contribution to the ANN output was given by the signals content in the low frequency range, especially into the downstream frequency contents.

Experiments pointed up a large influence of thermal effects in the transition to supercavitation, as shown in the flow pattern map (Tab. 1), and confirmed by the estimated temperature depression in the orifice at different cavitation numbers. This justifies the high impact of temperature on supercavitation prediction. In Fig. 4 the effectiveness factor of each input of the neural networks over the super cavitation, is shown.

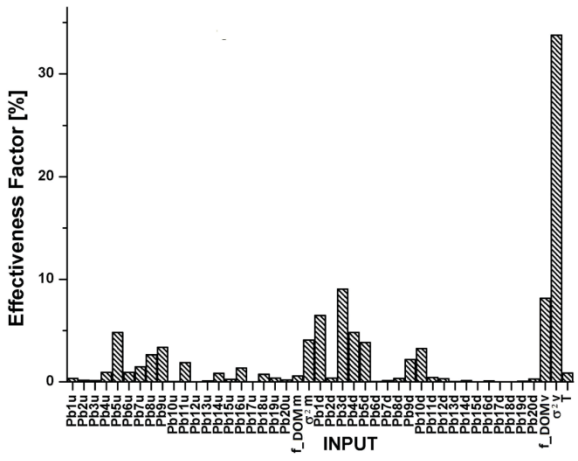

Fig. 3: Effectiveness factor of each input of the neural networks for all cavitation regimes

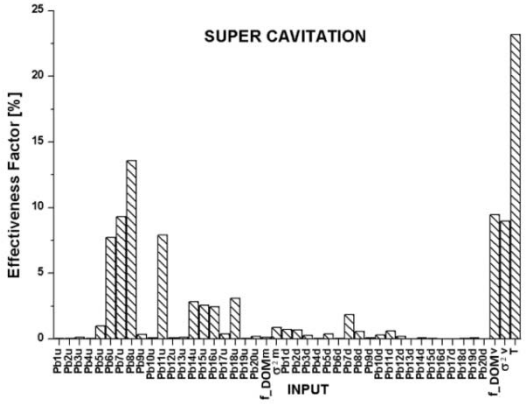

Fig. 4: Effectiveness factor of each input of the neural networks over the single data sets: Super cavitation.

5. CONCLUSIONS

In some cases, including hot fluid injection or cryogenic cavitation, fluid temperature has an high impact on cavitation development. In the present work an experimental study of a two-phase flow of water inside an orifice nozzle was performed. Using image and frequency analyses of the up- and downstream pressure signals, Four different regimes of the cavitation phenomena could be identified at different cavitation numbers. Different flow behaviors can be identified for varying pressures inside the orifice. Each behavior corresponds to a characteristic visible aspect of cavitation volume. Cavitation behavior was influenced both by the cavitation number and temperature. In particular transition to the supercavitation regime was more affected by temperature; the thermodynamic effects became more evident when the cavitation number was smaller.

At cavitation inception, the increase in the FFT amplitude of the upstream signal is most evident, especially in the high-frequency range, due to the growth and collapse of small cavities.

The transition to jet cavitation is characterized by a significant increase in FFT amplitude in the low-frequency range. For further cavitation number reductions, the spectra of the upstream signal show no evident peaks, and there is an increase in the FFT amplitude of the downstream signals in the 0-2000 *Hz* frequency range. A three-layer Elman neural network was designed, using as inputs the power spectral density distributions of dynamic differential pressure fluctuations, recorded downstream and upstream the restricted area of the orifice. Results show that the designed neural networks predict the cavitation patterns successfully comparing with the cavitation pattern by visual observation.

The Artificial Neural remarks also the impact that each input had in the training process, so it is possible to identify the frequency ranges that more influenced the different cavitation regimes and the impact of the temperature and the cavitation regime in which temperature is more relevant.

6. REFERENCES

[1] N. Tamaki, M. Shimizu, H. Hiroyasu, "Enhancement of the atomization of a liquid jet by cavitation in a nozzle hole", Atomization Sprays, vol. 11, no.2, pp. 125 – 137, 2001

[2] C. Soteriou, R. Andrews, , M. Smith, "Direct injection diesel sprays and the effect of cavitation and hydraulic flip on atomization", in: SAE 950080, pp. 128 – 153,1995.

[3] H. Hiroyasu, "Spray breakup mechanism from the hole-type nozzle and its applications", Atomization and Sprays, vol. 10, pp. 511 – 527, 2000.

[4] J. P. Franc, C. Rebattet, A. Coulon, "An experimental investigation of thermal effect in a cavitating inducer", ASME J. Fluids Eng. 126, pp. 716 – 723, 2003.

[5] H. A. Stahl, A. J. Stepanoff, N. J. Phillipsburg, "Thermodynamic aspects of cavitation in centrifugal pumps", ASME Journal of Basic Engineering, vol. 78 (8), pp. 1691 – 1693, 1956.

[6] N. Tani, T. Nagashima, "Cryogenic cavitating flow in 2d laval nozzle", Journal of Thermal Science, vol. 12, pp. 157 – 161, 2003.

[7] J. P. Gustavsson, K. C. Denning, C. Segal, "Hydrofoil cavitation under strong thermodynamic effect", ASME Journal of Fluids Engineering, vol. 130 (9) 091303 – 091308, 2008.

[8] M. Rodio, M. G. De Giorgi, A. Ficarella, "Influence of convective heat transfer modeling on the estimation of thermal effects in cryogenic cavitating flows", International Journal of Heat and Mass Transfer, vol. 55, pp. 6538 – 6554, 2012.

[9] B. Ji, X. Luo, X. Peng, Y. Wu, H. Xu, "Numerical analysis of cavitation evolution and excited pressure fluctuation around a propeller in non- uniform wake", International Journal of Multiphase Flow, vol.43, pp. 13 – 21, 2012.

[10] K. Sato, Y. Saito, "Unstable cavitation behavior in a circular-cylindrical orifice flow", JSME Int. J., Ser. B, vol. 45 (3), pp. 638 – 645, 2002.

[11] M. G. De Giorgi, D. Bello, A. Ficarella, "Analysis of thermal effects in a cavitating orifice using rayleigh equation and experiments", Eng.Gas Turb. Power vol. 134. pp. 092901(1) - 092901(10), 2010.

[12] M. G. De Giorgi, F. Chiara, A. Ficarella, D. Laforgia, "Experimental and numerical investigations of cavitating flows", in: Proceedings of 35th AIAA Fluid Dynamics Conference and Exhibit, AIAA, 2005.

[13] M. G. De Giorgi, M. G. Rodio, A. Ficarella, "Cavitation modeling in cryogenic fluids for liquid rocket engine applications", in: AIAA 38th Fluid Dynamics Conference and Exhibit, Seattle, WA, 2008.

[14] M. G. De Giorgi, A. Ficarella, M. Tarantino, "Evaluating cavitation regimes in an internal orifice at different temperatures using frequency analysis and visualization", International Journal of Heat and Fluid Flow, vol. 39, pp. 160 – 172, 2013.

[15] M. G. De Giorgi, A. Ficarella, M. Tarantino, "Error analysis of short term wind power prediction models", Applied Energy,vol. 88 (4), pp.1298 – 1311, 2011.

[16] M. G. De Giorgi, A. Ficarella, M. Tarantino, "Assessment of the benefits of numerical weather predictions in wind power forecasting based on statistical methods", Energy, vol. 36 (7), pp. 3968 – 3978, 2011.

[17] T. Xie, S. Ghiaasiaan, S. Karrila, "Artificial neural network approach for flow regime classification in gas-liquid-fiber flows based on frequency domain analysis of pressure signals", Chemical Engineering Science, vol. 59, pp.2241 – 2251, 2004.

[18] D. Shi, H. Zhang, L. Yang, "Time-delay neural network for the prediction of carbonation tower's temperature", IEEE Trans. Instrum. Meas. 52 (No. 8), pp. 1125 – 1128, 2003.